Available online at www.sciencedirect.com
SCIENCE DIRECT®
Computational Materials Science 34 (2005) 35–45
COMPUTATIONAL MATERIALS SCIENCE
www.elsevier.com/locate/commatsci

A method for retrieving temperature and microstructure dependent apparent yield strength for aluminium alloys

Z.L. Zhang [a,*], Ø. Gundersen [b], R. Aune [b], J. Ødegård [b], Ø. Grong [c]

[a] *Faculty of Engineering Science and Technology, Norwegian University of Science and Technology (NTNU), Richard Birkelands vei 1a, N-7491 Trondheim, Norway*
[b] *SINTEF Materials and Chemistry, N-7465 Trondheim, Norway*
[c] *Faculty of Natural Science and Technology, Norwegian University of Science and Technology (NTNU), N-7491 Trondheim, Norway*

Received 1 July 2004; accepted 18 October 2004

Abstract

Materials constitutive behaviour at high temperature is dependent on both temperature and microstructure. This paper presents a method to retrieve the temperature and microstructure dependent apparent yield strength of 6XXX aluminium alloys from the reaction force–temperature curves measured at the centre of the gauge length of a cylindrical specimen. The specimen is clamped at both ends and subjected to a controlled thermal history via induction heating. The experimental procedure is based on the test setup proposed by Satoh to determine residual stresses in welds. Various effects on the accuracy of the method have been investigated, including the effect of heating rate, hardening and testing frame stiffness. Examples have been shown for the aluminium alloy 6082 in T6 temper condition.

1. Introduction

The integrity of welded joints is strongly influenced by welding residual stresses [1,2]. Prediction of welding residual stresses involves description of highly complex thermo-metallurgical–mechanical phenomena—heat flow, microstructure evolution and plastic deformation [1–8]. For both steel and aluminium alloys the heat-affected-zone (HAZ) strength is a strong function of the resulting microstructure. Conventional analyses usually assume that material mechanical properties depend only on temperature [6,9,10]. Recently, progress has been made by Myhr and Grong [11–13] on modelling the microstructure evolution of 6XXX and 7XXX alloys. Microstructure dependent constitutive equations, though not described in detail, are also available [13]. These progresses pave the way for a better prediction of welding residual stresses in aluminium alloys. One important task

* Corresponding author. Tel.: +47 7359 2530; fax: +47 7359 4701.
E-mail address: zhiliang.zhang@ntnu.no (Z.L. Zhang).

0927-0256/$ - see front matter
doi:10.1016/j.commatsci.2004.10.004

remains is to calibrate the microstructure dependent constitutive equations and to develop a practical method for determining the temperature and microstructure dependent mechanical parameters.

In deriving such a method experience from conventional mechanical analysis can be borrowed. In mechanical analysis, the main input for strength analysis is material's true stress strain curve. The method for determining materials true stress strain curve is well-established, i.e., by testing smooth tensile specimen of circular or rectangular cross section [14,15], Fig. 1. Material's local stress strain curve can be retrieved from the global load versus diameter or thickness reduction curve of a tensile specimen [14,15].

In analogy to the mechanical problem, a similar method can be developed for determining the temperature and microstructure dependent apparent yield stress by using the Satoh test, Fig. 2. Satoh developed the test rig for assessing welding residual stress [16,17]. The test was performed by induction heating of a tensile specimen with both ends clamped. During the test, the reaction force-versus-temperature curves were recorded. The final reaction stress is the residual stress under constrained condition. The original Satoh test was designed for two purposes. First, for a given heat treatment, the Satoh test can be used for characterization of materials. Different materials for the same temperature history will result in different residual stress levels. Secondly, for a given material, the test can be used to study the effect of heat treatment.

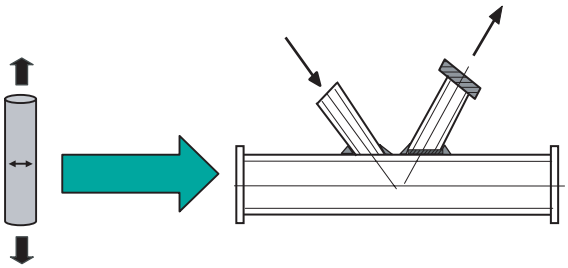

Fig. 1. Mechanical problem—material properties determined from simple tensile tests are transferred to structural analysis.

In this paper, the Satoh test is utilized for a different purpose. It is taken as a thermo-metallurgical tensile (TMT) test. A method has been developed to interpret the reaction force versus temperature curves and obtain microstructure dependent apparent yield stress data. The main challenge has been to determine which measured global quantities can be used to retrieve the local material parameters.

In the following, a general discussion of the constitutive behaviour is followed by a numerical study of the Satoh test. The relationship between the thermal history and reaction force in the Satoh test as well as the effect of several parameters including the test frame stiffness, strain hardening and heating rate has been investigated. Then, the results of an experimental Satoh testing program for a 6082 aluminium alloy in T6 temper condition are presented

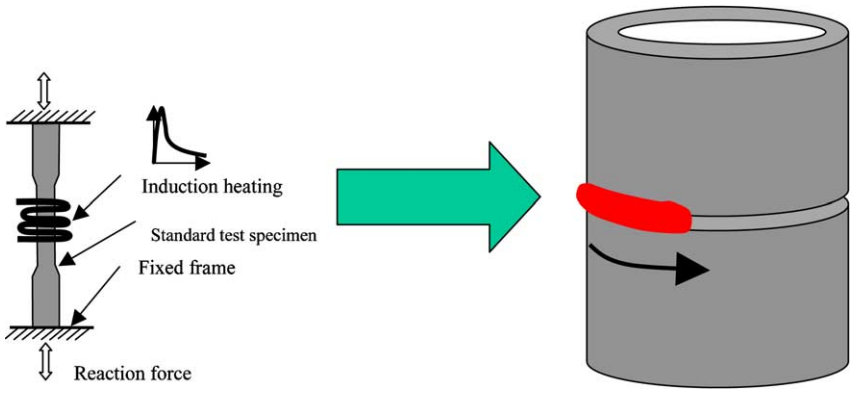

Fig. 2. Welding problem—temperature and microstructure dependent mechanical parameters from the simple Satoh test can be transferred to the analysis of complex weldments.

and analyzed. In the subsequent section, according to the Satoh concept, the temperature dependent apparent yield stress curves for different microstructure levels are constructed for the tested alloy. This paper is closed with discussions and general conclusions concerning the proposed method.

2. Constitutive behaviour

A constitutive equation links the strain to the stress at a material point. It describes the local material behaviour and is the most important part in welding mechanics [8]. For aluminium alloys, a constitutive equation can be written

$$\phi = q - \bar{\sigma}(\bar{\varepsilon}^p, T, m) = 0 \tag{1}$$

where q is the von Mises equivalent stress, $\bar{\sigma}$ is the current flow stress, $\bar{\varepsilon}^p$ is the equivalent plastic strain, T the temperature and m a microstructure parameter. For the microstructure model developed by Myhr and Grong [11–13], m is equal to, f/f_0 where f and f_0 are the current and initial volume fraction of hardening particles. Because m is a temperature history dependent parameter, Eq. (1) indicates that at the same temperature, for example, one before and one after the peak temperature, the material's yielding behaviour will be different. Eq. (1) has in fact neglected the strain rate effect, which could possibly influence the yielding behaviour [13]. There is, however, no strong indication on the importance of the strain rate effect in welding. For the sake of simplicity, the strain rate effect is not considered in the yielding behaviour in this study.

The plastic hardening behaviour at room temperature and high temperature are very different. Though for age hardening aluminium alloys, to some extent the underlying physical processes are well established, and kinetic models of precipitation coarsening and dissolution are available. However, there is almost no knowledge on the form of the hardening function and no method exists regarding how to determine the related constants. In general, both the yield stress and strain hardening ability are dependent on temperature and microstructure. This makes the expression of $\bar{\sigma}$ complicated. In this paper we treat the material behaviour at high temperature as elastic–perfectly plastic. By doing so, the $\bar{\sigma}$ in Eq. (1) can be replaced by the apparent yield stress

$$\bar{\sigma} = \bar{\sigma}_T(T, m) \tag{2}$$

The above equation is valid of course in an approximate sense. In the following, it will be shown that the non-hardening assumption may be a reasonable choice for the welding residual stress analysis, where plastic strain is generally small.

3. The Satoh concept

In the following, the behaviour of Satoh specimen will be studied in detail. The main question is whether and which output from a Satoh test can be converted back to the local material property. The procedure used is: for a given material curve (yield stress versus temperature curve), finite element analyses were carried out to calculate the global curves—reaction stress versus temperature curves. The calculated global curves are compared with the original material (input) curve. ABAQUS [18] was used in the analyses. In the numerical study, the effect of microstructure was not included.

Fig. 3 shows a sketch of the Satoh specimen used. The diameter of the specimen was chosen to prevent buckling during heating and to avoid

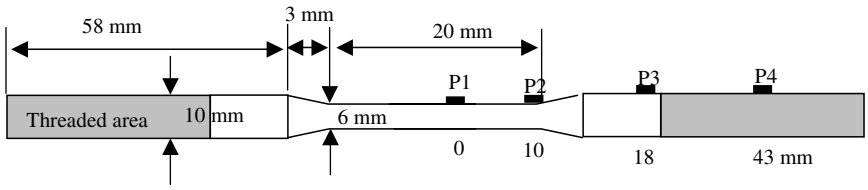

Fig. 3. The Satoh specimen and positions P1, P2, P3 and P4 for temperature measurement.

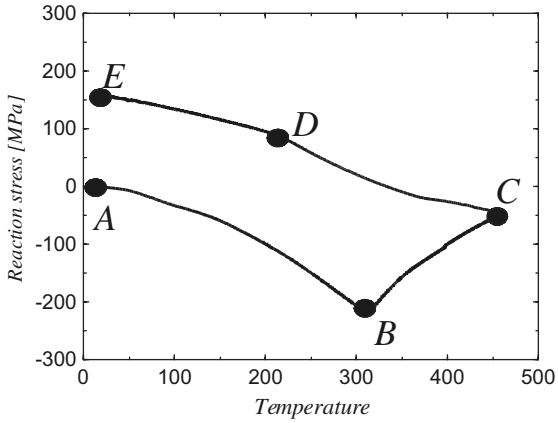

Fig. 4. Typical output curve from the Satoh test for aluminium alloys. The temperature is measured at the middle axial position of the specimen surface.

strong temperature gradients across the cross section. Fig. 4 shows the typical output from Satoh testing of aluminium alloys. The abscissa represents the temperature measured at a surface position on the Satoh specimen, and the ordinate is the reaction stress−reaction force divided by the initial minimum cross section of the specimen. During heating, the temperature increases and compressive stress builds up in the Satoh specimen. For aluminium alloys, the reaction force can usually be separated into four parts. From A to B, the behaviour of the specimen is thermal elastic with no plastic deformation. The curvature of segment AB is dependent on the Young's modulus E, Poisson ratio ν and thermal expansion coefficient α that are all a function of temperature, and also the frame stiffness. Detailed study on the curvature follows. When the temperature increases, the compressive stress also increases, but the yield strength will decrease. At about 300 °C, plastic yielding occurs. Part B to C involves both thermal plastic yielding and strain hardening, and also a strong change of the microstructure. Point C represents the peak temperature, after which the specimen will be cooled down by either forced or free cooling. During cooling, the material starts to contract and compressive stress is reduced. At a certain temperature, tensile stress begins to develop. Segment CD is similar to the segment A to B, where no plastic deformation occurs, but may involve a change of microstructure. At point D, plastic yielding starts again. In segment DE, plastic yielding is dominating. The stress level at point E is the final residual stress. This paper focuses on the plastic loading parts, BC and DE.

In this study, sequentially coupled analyses were carried out. First, thermal analyses were made to simulate the induction heating and free/forced cooling. The resulting temperature fields were used as the basis for the subsequent mechanical analysis. The heat generated by plastic deformation was neglected.

Fig. 5 shows the temperature history from the thermal analysis. The heating time used is 28 s [19]. The temperature dependence of Young's modulus, Poisson ratio and thermal expansion coefficient were taken from [4] and are listed in Table 1. The FE mesh (axisymmetric) used in the thermal- and mechanical analyses are identical and is shown in Fig. 6a. The element type for thermal analysis is DCCAX4 and for mechanical analysis is CAD4 [18]. As mentioned earlier, the Satoh frame is not fully rigid. In order to simulate the deformability of the Satoh frame a linear spring element in ABAQUS has been used. Fig. 6b shows the temperature dependent yield stress curve inputted in the FE analysis.

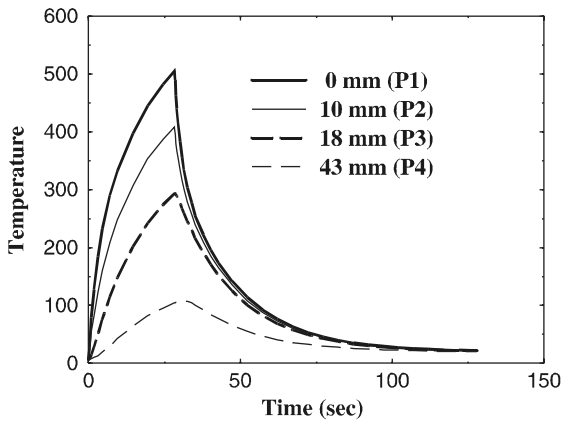

Fig. 5. Temperature histories from a thermal analysis which was then used for the mechanical analysis. The length in the legend indicates the axial surface location (shown in Fig. 3) where the temperature was measured.

Table 1
Mechanical constants as a function of temperature used in the mechanical analyses

Temperature T (°C)	Young's modulus E (Mpa)	Poisson ratio ν	Thermal expansion coefficient α (1/°C)
20	71,000	0.30	2.3×10^{-5}
200	60,000	0.31	
400	38,000	0.33	
550	5000	0.34	3.3×10^{-5}

As discussed in the previous section, a non-hardening plastic material model was used in the analyses. Fig. 7 compares the yield stress curve inputted to the analysis and the reaction stress versus temperature curves. The temperature was measured at the different locations along the specimen surface. Because the influence of microstructure was not considered in Fig. 7, the yield stress curve is symmetric, i.e., same temperature results in same yield stress. It should be noted that the yield stress curve represents the material local behaviour, while the curves from the Satoh test are the global averaged response of the specimen.

Fig. 7 indicates that there are great differences between the curves generated from temperatures measured at different locations along the Satoh specimen. Since induction heating is imposed only in the central part of the specimen, the temperature at a position as P4 will be significantly lower than the temperature in the middle of specimen (P1) during heating. The reaction stress versus temperature curve at P4 is away from the inputted material curve. That indicates that the global behaviour represented by the reaction stress versus temperature at P4 cannot be taken as the local material curve. This will be so for all Satoh curves

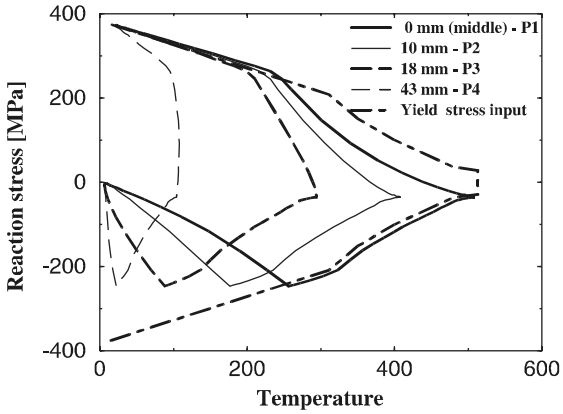

Fig. 7. Reaction stress as a function of temperature at different locations along the specimen. Both ends were fixed and non-hardening material was used in the analyses. The length in the legend indicates the distance from the middle of the specimen.

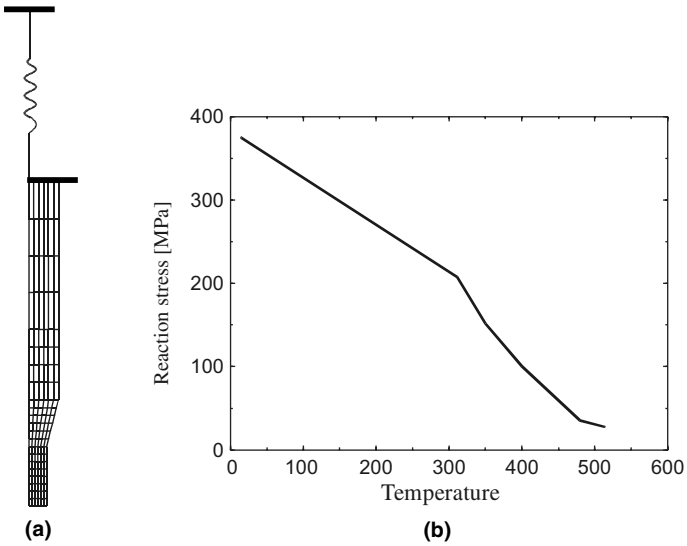

Fig. 6. (a) The mesh used in both the thermal and mechanical analyses. The mesh types are however, different; (b) temperature dependent yield stress inputted in the analyses.

generated by temperature measurements far away from the middle of the specimen. When the location moves close to the middle of the specimen, the temperature becomes higher. It can be noted that the plastic parts of the reaction stress–temperature curve at P1 is very close to the material curve. Furthermore, when the specimen cools down, all the measurements give identical representation of the material's local behaviour. This finding indicates that the BC and DE segments of a Satoh curve at P1 can be approximately taken as the local material behaviour, i.e., the material's temperature dependent yield stress.

The interesting observation lays down the Satoh concept, namely a special global curve from the test can be transferred to the local material behaviour. Satoh test can, therefore, be treated as a TMT test. Unlike the conventional tensile test, no correction such as the one by Bridgman for necking [14] may be needed. That means that the plastic parts of a Satoh test result can be directly used for welding residual stress analysis.

In the following, the effect of several factors on the accuracy of the method is studied, and the Satoh curve is defined as the reaction stress versus temperature curve measured at the middle of the specimen.

4. Parametric study

4.1. Effect of hardening

In the above analysis, the material has been assumed to be elastic–perfectly plastic. The hardening effect on the relationship between the Satoh curve and the material's local yielding behaviour has been investigated, and the results are shown in Fig. 8. A linear hardening law was used. The hardening was further assumed to be independent of temperature. The linear hardening modulus $H = \frac{d\sigma}{d\bar{\varepsilon}^p}$ varied from 0 (no hardening) to 400 MPa.

Fig. 8 shows that increasing hardening increases the gap between the global Satoh curve and the local material curve. If a real hardening material is modelled by a non-hardening plastic model, the finite element analysis will slightly underestimate the welding residual stress. However, when the plastic parts from a real Satoh test including the effect of hardening are taken as the material curve and a non-hardening material model is then used in subsequent analyses, the finite element prediction will be very close to the Satoh test results. As long as residual stresses are concerned, the material curve taken from the Satoh tests together with a non-hardening material model will give reasonably accurate prediction. The plastic deformation which occurred during welding depends on the geometry constraint enforced to the specimen. Satoh specimen represents one extreme. The maximum plastic strain experienced during the non-hardening analysis is about 16%. The plastic strain in a actual welding may be far below that value.

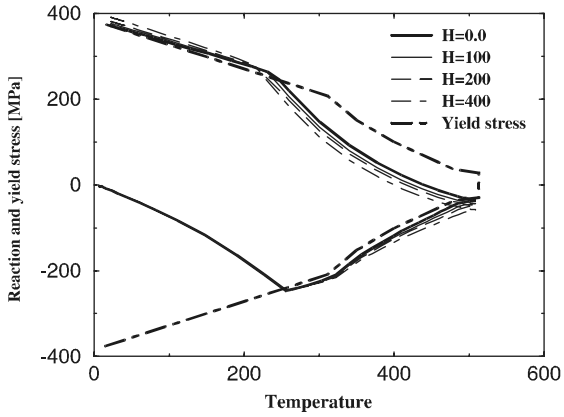

Fig. 8. Effect of hardening on the reaction stress versus temperature curves of Satoh specimens. "Yield stress" in the legend indicates the material curve inputted in the analysis.

It should be noted that the use of a non-hardening plastic model will not influence the occurring of material yielding in the Satoh test and the actual hardening will be somewhat decreased with increase in temperature. When the peak temperature is high enough, the plastic deformation history accumulated during heating will disappear.

4.2. Effect of stiffness

The ideal situation is that both ends of the Satoh specimen are clamped. However, in real tests, the frame of the test rig is not fully rigid. Furthermore, mounting of the specimen is usually not perfect. There is often a certain amount of

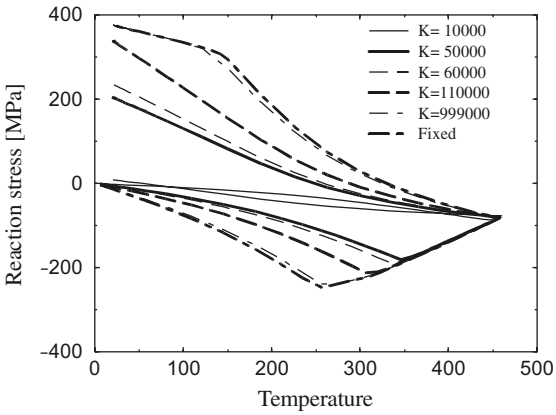

Fig. 9. Effect of stiffness on the Satoh reaction curve. A low stiffness leads to a delayed plastic response during heating and cooling. No-hardening material was used in the analyses.

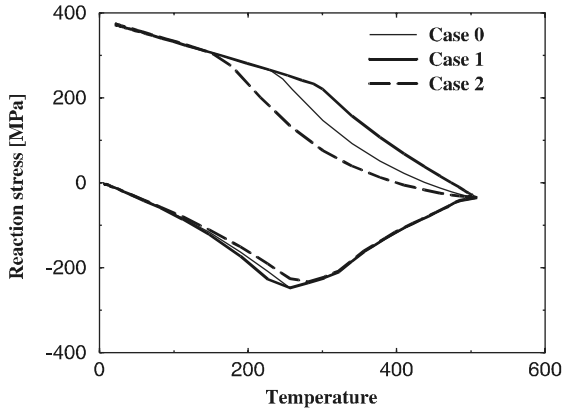

Fig. 10. Effect of thermal constants on the Satoh curve. In case 0, all the constants are dependent on temperature, in case 1 only the thermal coefficient is dependent on temperature, while in case 2 both the Young's modulus and Poisson ratio are dependent temperature.

gliding in the beginning of the test. Different stiffness of the spring elements has been applied to investigate this effect. Fig. 9 shows the reaction curves for six cases. It can be seen that a smaller stiffness will reduce the reaction stress at a given temperature and delay the plastic yielding. When the stiffness is small enough, there is nearly no reaction stress. This observation reminds us that welding residual stress is strongly related to the geometric constraint enforced to the specimen.

It is interesting to note from Fig. 9 that, once the plastic yielding has started, the yielding behaviour of a non-hardening material is not influenced by the stiffness any more. The stiffness of the Satoh frame (K) used in this paper has been measured and found to be 110,000 N/mm. Because of the gliding of the specimen during the early stage of loading, the effective stiffness will be lower than the measured one. Fig. 9 shows that when the K approaches 1,000,000 N/mm, the Satoh frame is almost rigid.

The general conclusion from Fig. 9 is that the Satoh frame stiffness will affect the temperature range where plastic deformation occurs. However, it will not significantly influence the plastic yielding behaviour.

4.3. Effect of thermal constants

The effect of Young's modulus, Poisson ratio and thermal expansion coefficients on the Satoh results has also been studied. Fig. 10 gives a comparison of the results of three cases. A non-hardening material was considered. In case 0, Young's modulus, Poisson ratio and thermal expansion coefficient are all dependent on temperature. The dependence is shown in Table 1. In case 1, the Young's modulus E and Possion's ratio v were kept constant (taken the value at room temperature), while in case 2 the thermal expansion coefficient is taken as constant. It can be observed from Fig. 10 that the curvature of the elastic parts are strongly affected by the thermal constants, however, once plastic yielding has started, it will dominate the response. The range of plastic deformation will also be dependent on the thermal constants.

4.4. Effect of heating rate

The heating time in all the previous analyses was 28 s which was taken from the experiments [19]. In order to study the effect of heating rate, another case with heating time 2.8 s has been analyzed. The peak temperature and cooling rate (free cooling) were identical to the previous case. Fig. 11 shows the effect of heating rate on the resulting Satoh curves. It should be noted that the temperature displayed in the figure was measured on the specimen surface.

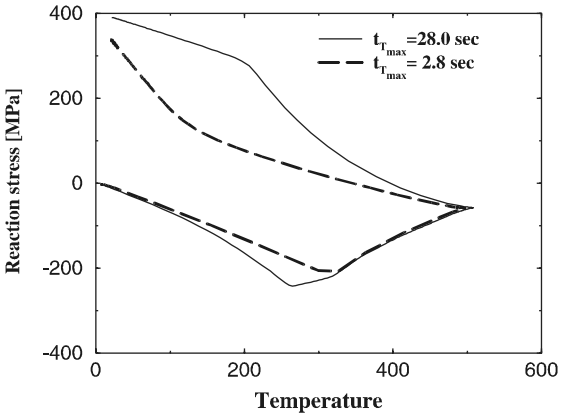

Fig. 11. The effect of heating time.

When the heating rate is slow, the temperature across the cross section is uniform and the gradient between the specimen centre and surface is very small. However, in the fast heating case, the gradient across the section and along the axial direction is much greater than in the slow heating case. It can be seen from Fig. 11 that the specimen with fast heating will enter into the plastic deformation phase at a later stage than the slow heating. However, once in the plastic deformation process, the plastic response of both cases is the same. When the central part of the fast heating specimen starts to cool down, the neighbouring part of the specimen may still be in high temperature, which indicates the fast heating specimen in a average sense may not enter the plastic deformation process again. The conclusion from Fig. 11 is that faster heating reduces the valid range of plastic deformation and may not be a good choice for Satoh testing. Nevertheless the recorded yield strength if any should be valid.

5. Application of the Satoh concept to the AA6082 T6 alloy

5.1. Experimental program

A testing program has been carried out to verify the Satoh concept. The material tested was a 6082 T6 aluminum alloy. The chemical composition of the alloy is shown in Table 2.

The testing program includes different peak temperature and cooling rates. Both free cooling and forced cooling have been used. It has been found that both free cooling and forced cooling give nearly identical results [19].

Table 2
The chemical composition of the 6082 T6 alloy (in wt%)

Alloy	Si	Mg	Mn	Cr	Fe
AA6082 T6	1.13	0.90	0.64	0.12	0.43

Fig. 12a shows the experimental Satoh curves where one loop represents one test with a particular peak temperature. The peak temperature varied from 150 to above 500 °C. The alloy starts to yield when the temperature is above 300 °C and the maximum compressive stress measured is about 200 MPa. When the peak temperature is below 300 °C, no plastic deformation occurred and no final residual stress was recorded. In this case heating and cooling paths composed a closed loop.

It is interesting to observe that the plastic yielding part during heating follows a "unique" curve. Different peak temperatures result in, however, different yielding behaviour in the cooling part. It is obvious that for the same temperature level, the plastic yielding is strongly non-symmetric. It must be noted that high peak temperature will give a lower residual stress level as compared to the cases with a reduced peak temperature. This can be explained by the fact that the microstructure for the high peak temperature case is different (lower volume fraction of hardening particles) to the case where the peak temperature is low. Some of the specimens used in the tests have been further tested at room temperature by tensile testing. The results are shown Fig. 12b.

5.2. Calculation of microstructure

Knowledge of the microstructure composition at position P1 is essential to retrieve the microstructure dependent apparent yield strength. Myhr and Grong's microstructure model for aluminium alloys 6082 in T6 temper condition [11,12] has been used to calculate the microstructure composition. In the model, the microstructure composition is represented by the relative volume fraction ratio

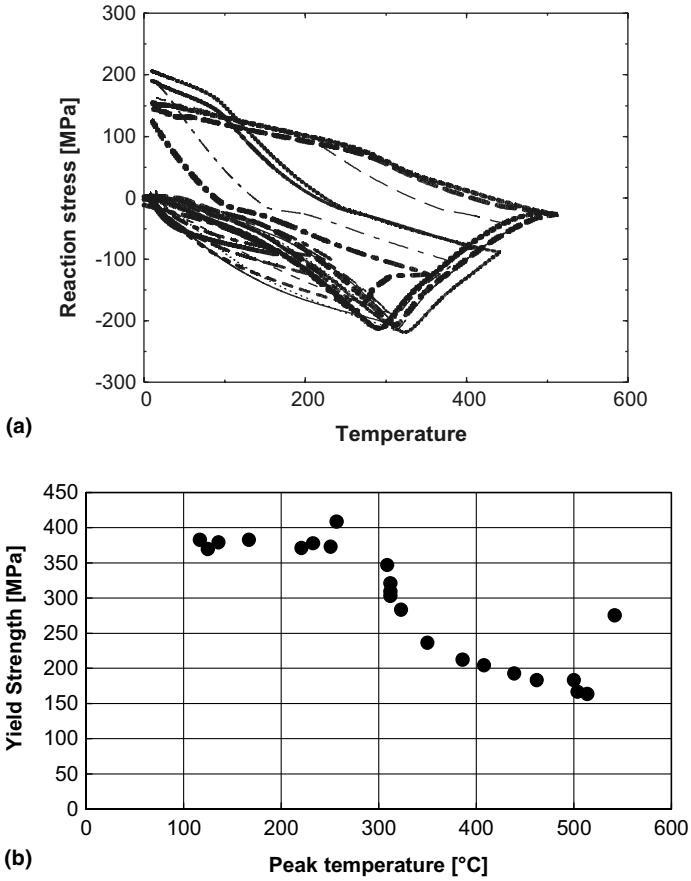

Fig. 12. (a) Experimental Satoh curves of a aluminium alloy 6082 in T6 temper condition where each loop represents one test with a particular peak temperature; (b) room temperature yield stress as a function of peak temperature in the Satoh test.

f/f_0 of hardening particles, where f and f_0 are the current and initial volume fractions, respectively. Detailed description of the microstructure model can be found in [11,12].

Fig. 13 shows the predicted microstructure versus peak temperature for the tested alloy. It can be seen that for the heating conditions applied, microstructure decomposition commences at a temperature of 230 °C. This behaviour is qualitatively in accord with the results shown in Fig. 12b where the apparent yield strength at room temperature starts to decay when the peak temperature is higher than 250 °C. The microstructure calculations in Fig. 13 also show that a complete dissolution of the hardening particles is achieved at a peak temperature of 460 °C.

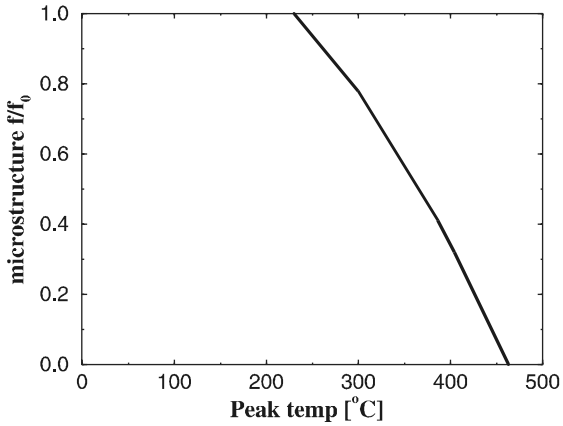

Fig. 13. Scaled volume fraction of hardening precipitates as a function of peak temperature. Microstructure was assumed to be constant during cooling.

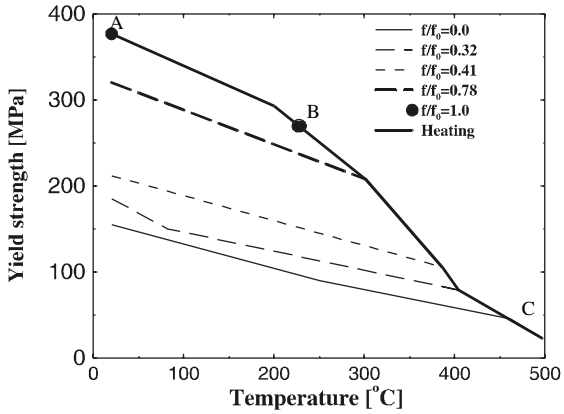

Fig. 14. Retrieved apparent yield strength of the aluminium alloy 6082 T6 as a function of temperature for different microstructure compositions.

5.3. Determination of temperature dependent apparent yield strength for different microstructure compositions

From the Satoh test results, Fig. 12a, we can first retrieve the apparent yield strength versus peak temperature curve, BC in Fig. 14. Then by neglecting the microstructure change during the cooling, and utilizing the tensile test results at room temperature Fig. 12b, and microstructure data, Fig. 13, we can obtain the whole set of apparent yield stress versus temperature curves for different microstructure compositions, Fig. 14. Point B indicates where the microstructure starts to change once the peak temperature is higher than this point. When the peak temperature is below point B, during the heating and cooling, yielding will follow the same path. However, when the peak temperature is within the segment BC, material yielding during cooling and heating will take different paths. For the same temperature, the yield stress at heating is much higher than that at cooling. Fig. 14 represents the complete yield behaviour of the tested alloy, and can be used for calibration of constitutive equations.

6. Concluding remarks

Inspired by the conventional tensile testing for determining materials' true stress–strain curves, in this paper, a simple method based on the Satoh concept has been explored for retrieving the microstructure dependent apparent yield stress versus temperature curves. By an extensive numerical study of the Satoh test, it has been found that, by measuring the reaction stress and the temperature in the middle specimen, the resulting reaction curve can be directly taken as the local material curve. The specific design of the Satoh test specimen should prevent thermal buckling and minimize the temperature gradient across the section.

Various effects on the accuracy and valid range of the method have been investigated. It has been shown that testing frame stiffness, heating rate, thermal constants as well as hardening ability will mostly influence the valid range of the resulting data, not the accuracy of the method. The method has been applied to the aluminium alloy 6082 T6. A complete set of the alloy's microstructure dependent apparent yield strength versus temperature data has been presented.

It must be noted that the proposed method is simple and approximate in nature. It has been argued that the assumption of a non-hardening plastic model will not induce significant error in welding residual stress analysis. The Satoh specimen represents one extreme case of welding uniaxial stressing and very low geometry constraint. Welding of (thick) plates often involve three-dimensional stresses and high geometry constrain, and, therefore, less plastic deformation. This indicates that the strain hardening effect may be less significant in real welding than in the Satoh tests. If for materials with which high temperature hardening models are nevertheless available, these models can be incorporated in the method. The proposed method can also be applied to more advanced testing techniques, such as the Gleeble welding thermal simulation technique, where multiaxial loading is possible during thermal simulation, and thus, better valid range and better accuracy may be achieved.

The strength loss of the aluminium alloy shown in the paper is not permanent, but will gradually become smaller as excess solute starts to recombine and form GP-zones during subsequent natural aging. This recovery process is not included in this study. It must be noted that strain rate effect

has been neglected in the study. The effect of strain rate on the plastic flow is generally regarded as not significant in welding. However, true understanding of the strain rate effect in welding of aluminium alloys certainly deserves further efforts.

In principal, the proposed method can be applied to welding of steel. Some precautions should, however, be made. Metallurgical phenomena in steels are generally more complex than in aluminium alloys, in particular, phase transformation during heating and cooling should be considered.

Acknowledgment

The financial support from the Norwegian Research Council via a Strategic Institute Program (SIP) is greatly appreciated.

References

[1] P. Dong, F.W. Brust, Welding residual stresses and effects on fracture in pressure, vessel and piping components: a millennium review and beyond, J. Pressure Vessel Technol. 122 (2000) 329.

[2] G. Bussu, P.E. Irving, The role of residual stress and heat affected zone properties on fatigue crack propagation in friction stir welded 2024-T351 aluminium joints, Int. J. Fatigue 25 (2003) 77–78.

[3] M. Peel, A. Steuwer, M. Preuss, P.J. Withers, Microstructure, mechanical properties and residual stresses as a function of welding speed in aluminium AA5083 friction stir welds, Acta Mater. 51 (2003) 4791–4801.

[4] D. Radaj, H. Hauser, S. Braun, Numerical simulation of residual stress and distortion of welded joints in 6XXX alloys, Konstruktion 50 (1998) 30–38.

[5] J.A. Free, R.F.D.P. Goff, Predicting residual-stresses in multi-pass weldments with the finite-element method, Comput. Struct. 32 (1989) 365–378.

[6] J. Cañas, R. Picón, F. Pariís, A. Blazquez, J.C. Marín, A simplified numerical analysis of residual stresses in aluminum welded plates, Comput. Struct. 58 (1996) 59–69 (No microstructure was considered).

[7] L.E. Lindgren, A. Oddy, Toobox for computing phase transformations and material properties of hypoeutectoid steels in Satoh test, First International Symposium on Thermal Stress and Related Topics, Japan, June 5–7, 1995.

[8] H. Murakawa, Computational welding mechanics and its interface with industrial application, International symposium on Theoretical Prediction in Joining and Welding, JWRI, Osaka University, Japan, 1996.

[9] X.K. Zhu, Y.J. Chao, Effects of temperature-dependent material properties on welding simulation, Comput. Struct. 80 (2002) 967–976.

[10] G.H. Little, A.G. Kamtekar, The effect of thermal properties and weld efficiency on transient temperatures during welding, Comput. Struct. 68 (1998) 157–165.

[11] O.R. Myhr, Ø. Grong, Process modelling applied to 6082-T6 aluminium weldments, Acta Metall. Mater. 39 (1991) 2093–2702;
O.R. Myhr, Ø. Grong, Process modelling applied to 6082-12 aluminium weldments, Acta Metall. Mater. 39 (1991) 2703–2708.

[12] O.R. Myhr, Ø. Grong, S.J. Andersen, Modelling of the age hardening behaviour of almgsi alloys, Acta Mater. 49 (2001) 65–75.

[13] O.R. Myhr, S. Klokkehaug, H.G. Fjaer, G. Grong, A.O. Kluken, Modelling of microstructure evolution and residual stress in processing and welding of 6082 and 7108 aluminium alloys, Proceedings of the Fifth International Conference on Trends in Welding Research, Georgia, USA, 1–5 June, 1998, pp. 233–238.

[14] Z.L. Zhang, M. Hauge, J. Ødegård, C. Thaulow, Determining material true stress strain curve from tensile specimens with rectangular cross section, Int. J. Solids Struct. 36 (1999) 3497–3516.

[15] Z.L. Zhang, J. Ødegård, O.P. Søvik, Determining true stress–strain curve for isotropic and anisotropic materials with rectangular tensile bars: method and verifications, Comput. Mater. Sci. 20 (2001) 77–85.

[16] K. Satoh, Transient thermal stress of weld heat affected zone by both-ends-fixed bar analogy, Trans. Jpn. Weld. Soc. 3 (1972) 125–134.

[17] K. Satoh, Thermal stresses developed in high-strength steels subjected to thermal cycles simulating weld-affected zone, Trans. Jpn. Weld. Soc. 3 (1972) 135–142.

[18] ABAQUS User's manual, V6.3 2002.

[19] R. Aune, Satoh testing of the aluminium alloy AA6082 (T4 and T6 temper conditions), SINTEF Report STF24 A99221, 1999.